Supporting Information

Torbati et al. 10.1073/pnas.1604777113

Methods

We model a bilayer as a 2D surface ω. The strain-energy density W for isotropic membranes is dependent on the mean curvature and the Gaussian curvature (16, 17, 48–52). Equilibrium configurations render stationary the augmented energy functional

$$E = \int_{\omega} [W(H,K;\theta^{\alpha}) + \lambda da - pV, \qquad \textbf{[S1]}$$

where λ and p are the Lagrange-multiplier fields associated with the area and volume constraints (53–55).

For the well-known Helfrich–Canham energy $W = kH^2 + \bar{k}K$ (16, 17), the equilibrium equation reduces to

$$k\left[\Delta H + 2H\left(H^2 - K\right)\right] - 2\lambda H = p. \qquad \textbf{[S2]}$$

We simulate axisymmetric geometries parametrized by meridional arclength s and azimuthal angle θ. Thus,

$$\mathbf{r}(s,\theta) = r(s)\mathbf{e}_r(\theta) + z(s)\mathbf{k}, \qquad \textbf{[S3]}$$

where $r(s)$ is the radius from the axis of symmetry and $z(s)$ is the elevation above a base plane. Because $(r')^2 + (z')^2 = 1$ there is an angle $\psi(s)$ such that

$$r'(s) = \cos\psi \quad \text{and} \quad z'(s) = \sin\psi. \qquad \textbf{[S4]}$$

The mean and Gaussian curvatures in the axisymmetric setup are given by (54, 55)

$$H = \frac{1}{2r}\{r\psi' + \sin\psi\}, \qquad \textbf{[S5]}$$

$$K = H^2 - \left(H - r^{-1}\sin\psi\right)^2. \qquad \textbf{[S6]}$$

The equilibrium equation (Eq. **S2**) simplifies to

$$L' = r\left[p/k + (2\lambda/k)H - 2H\left(H - r^{-1}\sin\psi\right)^2\right], \qquad \textbf{[S7]}$$

where

$$H' = r^{-1}L. \qquad \textbf{[S8]}$$

To compute the equilibrium geometry we solve the system of equations comprising **S4** (both parts), **S5**, **S7**, and **S8** for the unknowns r, z, ψ, H, and L. To solve these equations, we prescribe the following five boundary conditions at the two ends of the simulation domain as shown in Fig. 1:

i) For the near end at $r = 42.5$ nm:

$$r = 42.5 \text{ nm}, \quad \psi = \pi/2, \quad \text{and} \quad z = 0 \text{ nm}. \qquad \textbf{[S9]}$$

ii) For the far end:

$$\psi = 0, \quad \text{and} \quad L = 0. \qquad \textbf{[S10]}$$

The last condition arises from the equilibrium and the periodicity requirements and is equivalent to a clamped roller support.

We solve the set of ordinary differential equations along with the boundary conditions in MATLAB using "bvp4c solver." We simulated the effects of the mechanical state of the membrane, defined by the in-plane stress (λ, also called tension) and the out-of-plane stress (p, also called pressure) on the bilayer geometry. We perform these simulations for different bilayer sizes.

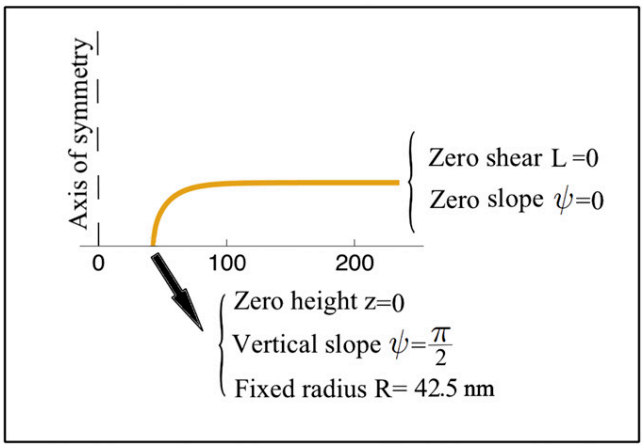

Fig. S1. Prescribed boundary conditions for the simulation of an axisymmetric bilayer.

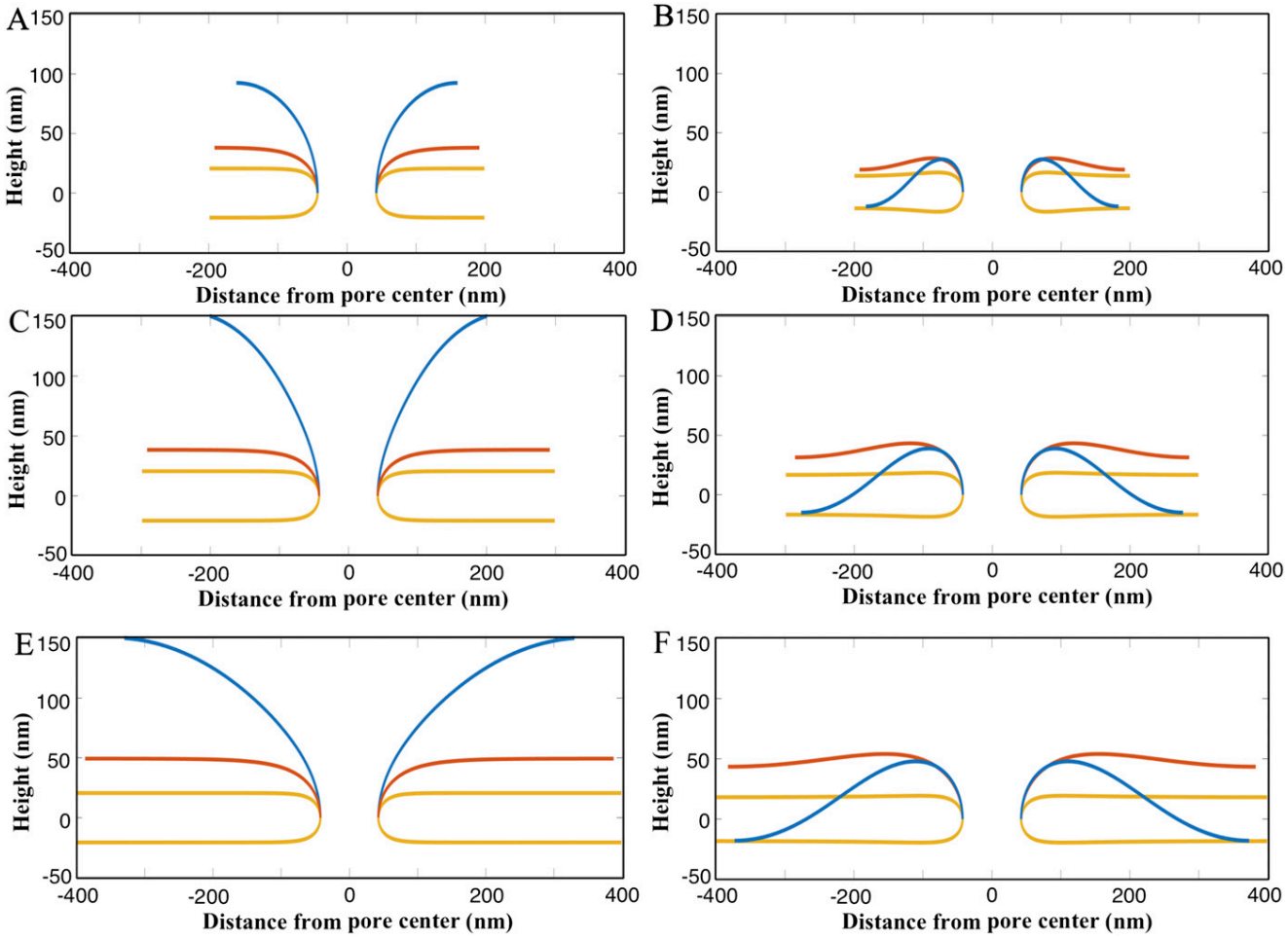

Fig. S2. Deflection response due to a reduction in the in-plane stress for (*A*) a 200-nm-radius bilayer at $p = 0$; (*B*) a 200-nm-radius bilayer at $p = 63.1$ Pa; (*C*) a 300-nm-radius bilayer at $p = 0$; (*D*) a 300-nm-radius bilayer at $p = 10.6$ Pa; (*E*) a 400-nm-radius bilayer at $p = 0$; and (*F*) a 400-nm-radius bilayer at $p = 3.02$ Pa.

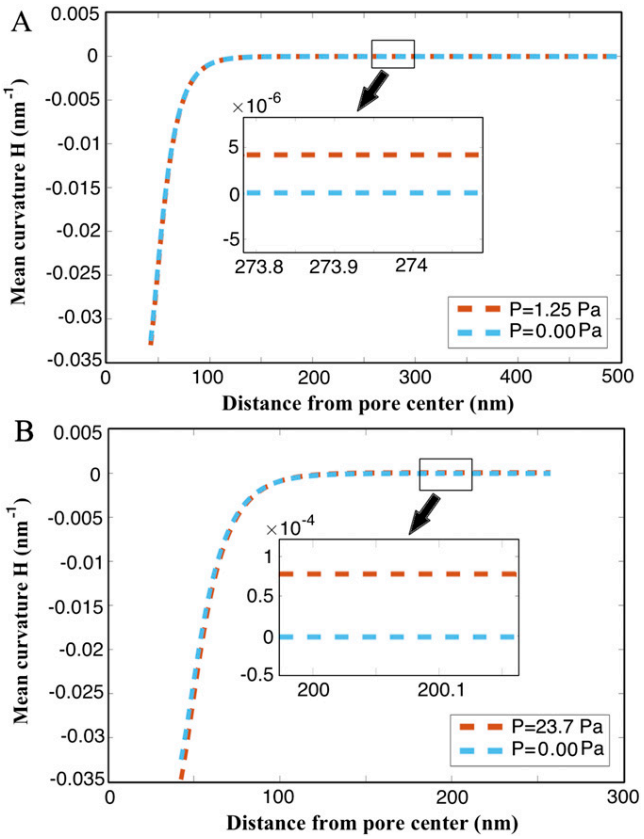

Fig. S3. Mean curvature variation along the bilayer for (*A*) a 500-nm-radius patch size and 0.15-mN/m in-plane stress and (*B*) a 250-nm-radius patch size and 0.15-mN/m in-plane stress.

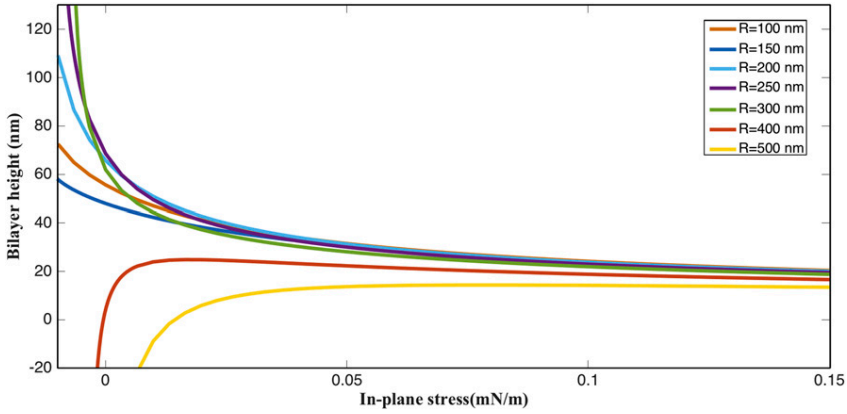

Fig. S4. Deflection response of the bilayers with different radii for a nominal $p = 5$ Pa. Bilayers with radii equal and smaller to 300 nm continue to expand out and do not undergo instability. In contrast, bilayers with 400- and 500-nm radii undergo buckling instability. Also note that the bilayer with $R = 500$ nm undergoes instability at tensile in-plane stress. This shows the high vulnerability of larger bilayers (~500-nm radius) to in-plane stress reduction.

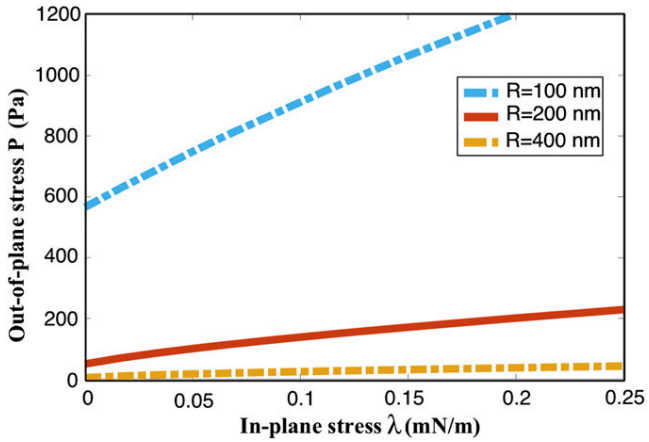

Fig. S5. Magnitude of out-of-plane stress (*p*) required to bend the membrane to fusion point for a range of positive in-plane stress values. For every size, a bilayer can undergo inward deformation even in the presence of tensile in-plane stresses due to the applied out-of-plane stress.

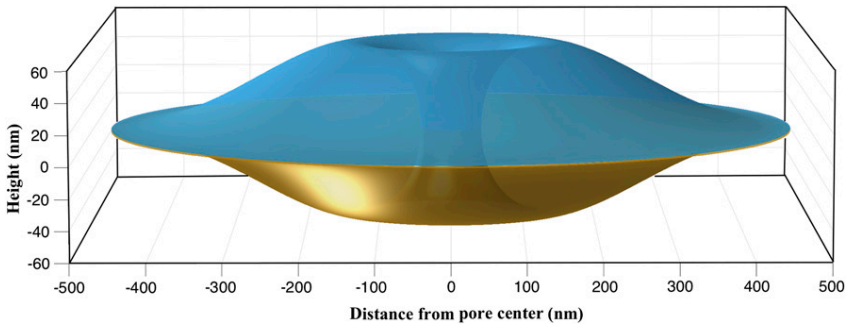

Fig. S6. Three-dimensional geometry of the buckled bilayer. In this scenario we assume both bilayers are buckling toward each other. This does not influence the stresses required to buckle because of the sharp decrease in the bilayer height near the critical point.

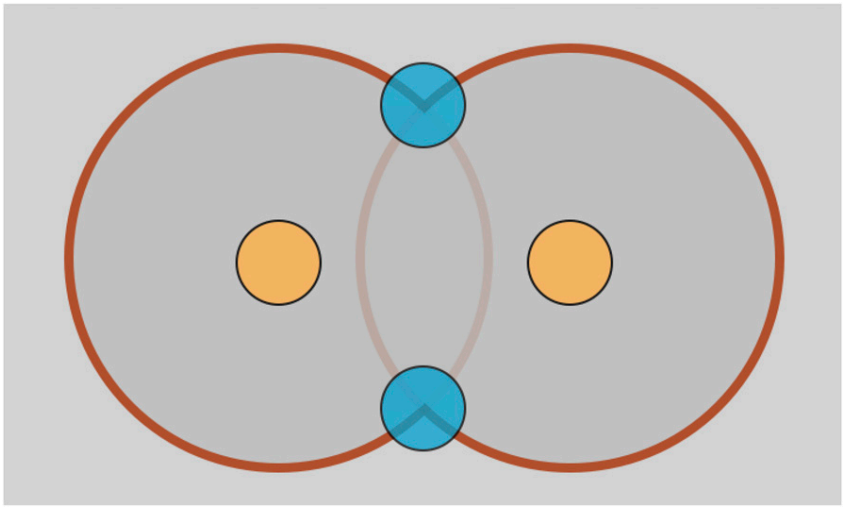

Fig. S7. Figure showing the interaction of fusion domains around two neighboring pores (shown in yellow). The blue regions indicate the hot spots at the interaction of two fusion domains. The inner radius of the red annulus indicates the predicted critical length scale that determines the pore separation. The width of the red annulus is controlled by the density of the existing pores. If the density is high, the width is small, and if the density is low, the width is large, leading to a bigger fusion domain where the two membranes meet.

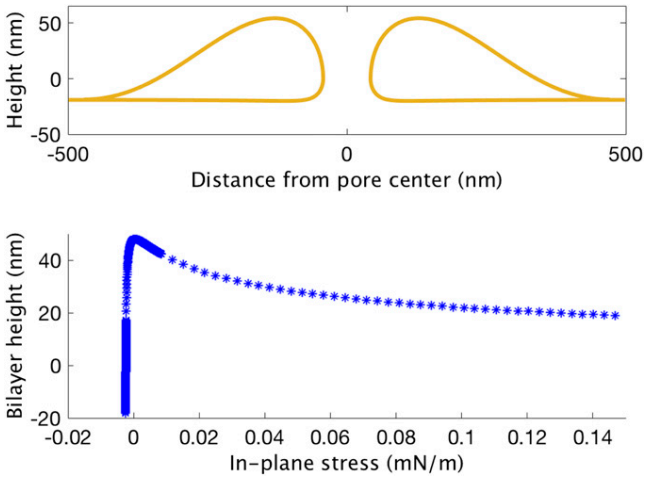

Movie S1. Inward buckling instability undergone by the outer bilayer due to a reduction in the in-plane stress.

Movie S1

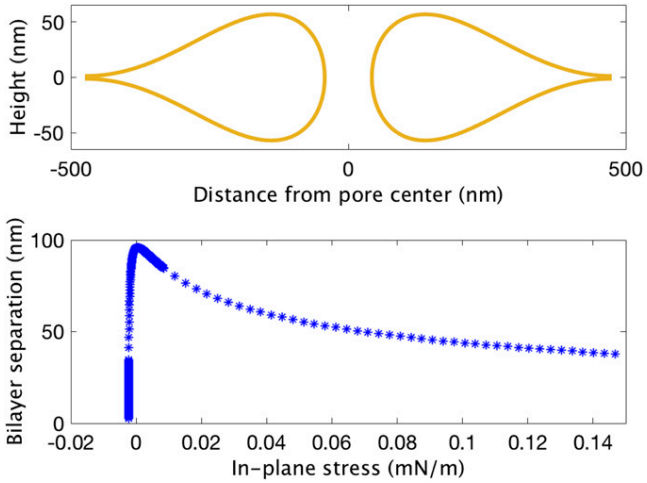

Movie S2. Inward buckling instability undergone by the outer and the inner bilayers due to a reduction in the in-plane stress.

Movie S2

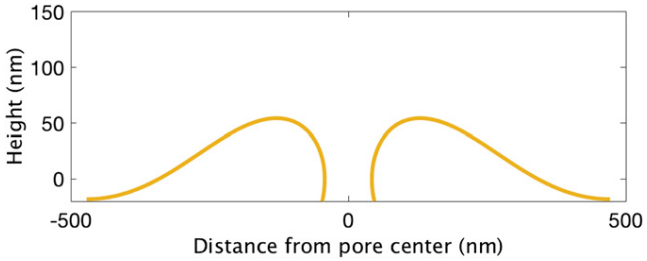

Movie S3. Inward buckling instability undergone by the outer bilayer due to areal growth. The in-plane stress is held at a fixed value.

Movie S3